Applied Catalysis B: Environmental 104 (2011) 282–290

Contents lists available at ScienceDirect

Applied Catalysis B: Environmental

journal homepage: www.elsevier.com/locate/apcatb

TiO_2 nanocrystals grafted on macroporous silica: A novel hybrid organic–inorganic sol–gel approach for the synthesis of highly photoactive composite material

Maurizio Crippa[a,*], Emanuela Callone[b], Massimiliano D'Arienzo[a], Klaus Müller[b], Stefano Polizzi[c], Laura Wahba[a], Franca Morazzoni[a], Roberto Scotti[a]

[a] Department of Materials Science, University of Milano Bicocca,Via R. Cozzi 53, Milano I-20125, Italy
[b] Department of Materials Engineering and Industrial Technologies, University of Trento, Via Mesiano 77, Trento I-38100, Italy
[c] Department of Physical Chemistry, Università Ca' Foscari Venezia, Via Torino 155/b, Venezia I-30172, Italy

ARTICLE INFO

Article history:
Received 21 January 2011
Received in revised form 4 March 2011
Accepted 12 March 2011
Available online 23 March 2011

Keywords:
Photoactivity
Organic–inorganic hybrids
TiO_2–SiO_2 composite
Hierarchical porous material

ABSTRACT

TiO_2–SiO_2 composite materials with photocatalytic properties similar to those of slurry powdered TiO_2 is obtained by a novel sol–gel synthetic strategy involving the hydrolysis/condensation of TMOS assisted by PEG as templating agent and the grafting of preformed titania nanocrystals onto the macropore walls of the silica matrix. In order to anchor TiO_2 particles to the surface of SiO_2, avoiding their embedding into silica matrix, functionalization with carboxylic acid or amine derivatives was carried out. The functionalization induces the confinement of titania nanocrystals in PEG, during the silica formation, and allows their dispersion on the silica surface. TiO_2–SiO_2 materials exhibit high thermal and chemical stability and a photocatalytic activity in the phenol mineralization comparable to that of powder TiO_2 in slurry (half degradation time ~120 min). These results suggest that the immobilization procedure here reported provides high accessibility of the catalyst active sites preserving the functional properties of the photoactive catalyst.

1. Introduction

In the last few years nanocrystalline TiO_2 has been extensively studied as the photocatalyst in the oxidative degradation of organic and inorganic pollutants [1]. The interaction of this oxide with UV radiation generates electron–hole pairs which are able to activate surface reactive processes [2]. The recombination rate of charges, which affects catalyst photoactivity, strongly depends on the morphological and structural properties of the oxide, such as the different crystalline phase, surface area, particle shape and porosity [3]. Consequently, the control of the photocatalytic activity of TiO_2 nanoparticles throughout the tailoring of their morphological and structural properties is a current topic of great interest.

The photodegradation of toxic compounds is usually performed by using titania nanoparticles in aqueous suspension (slurry). However, the use of nanosized powders as slurries in wastewater treatment causes difficult post-use recovery and requires expensive and time-consuming separation/recycling processes [4]. In addition, TiO_2 nanoparticles, when dispersed in the surrounding environment, may be hazardous, due to their potential inflammatory and cytotoxic effects [5]. These drawbacks can be avoided by immobilizing or embedding the TiO_2 nanoparticles on a support. Many inorganic or polymeric materials have been employed for this purpose: silica glass shaped as beads [6], rings [7], reactor walls [8] and fibers [9]; quartz [10]; zeolites [11]; perlite [12]; pumice [13]; alumina-based ceramics [14]; stainless steel [15]; aluminium [16]; cotton fibers [17]; polyester, acrylate [18], fluorinate [19] polymers. Nevertheless, both immobilization and embedding frequently lower the catalyst exposed area compared to that of the powder suspension [20].

Polymeric substrates show poor resistance to thermal treatments and undesired sensitivity to photooxidative processes, compared to inorganic ones [20b]. Inorganic membranes, consisting of macroporous ceramic substrates covered by micro/mesoporous active TiO_2 layers, seem promising alternatives for several large scale catalytic processes [21]. In fact, the porous skeleton of the ceramic framework provides chemical and thermal stability, mechanical durability, low pressure drops and rapid mass transport of fluids, due to the extensive interconnection between

* Corresponding author. Tel.: +39 02 64485027; fax: +39 02 64485400.
E-mail addresses: maurizio.crippa@mater.unimib.it, maurizio.crippa@unimib.it (M. Crippa).

0926-3373/$ – see front matter © 2011 Elsevier B.V. All rights reserved.
doi:10.1016/j.apcatb.2011.03.018

the macropores. This structure guarantees high accessibility to the catalyst active sites and fast uptake/release cycles. In addition, the mesoporosity of the titania layer preserves the permeability of the ceramic matrix and provides an effective contact between the target molecules and the catalyst particles [22].

Different approaches, based on soft-chemistry routes, hydrothermal synthesis, and chemical (CVD)/physical (PVD) vapour deposition, were proposed in order to obtain oxide coatings on preformed macroporous ceramic matrices [23]. The ideal active layers should be homogeneous, chemically and thermally stable, loading large amounts of material crucial for the catalytic activity and without pore occlusion which limits the whole permeability.

In this context, we propose a novel sol–gel synthetic strategy, employing hybrid organic–inorganic reactants for the preparation of a macroporous silica matrix and the simultaneous surface grafting of preformed TiO_2 nanocrystals. The goal is to design a TiO_2–SiO_2 (TS) composite material with the following characteristics:

- high macroporosity and UV-transparency of the silica matrix, which guarantee easy accessibility of the catalyst surface sites and allow effective interaction of TiO_2 with UV radiation;
- TiO_2 nanocrystals grafted on the surface of the ceramic matrix, whose well defined morphological and structural properties determine high photoactivity;
- minimum loss of photoactivity due to catalyst immobilization, in comparison to the slurry TiO_2;
- improved thermal stability and durability without leaching of the grafted catalyst.

The macroporous silica network was produced by the sol–gel process based on hydrolysis and condensation of tetramethylorthosilicate (TMOS) in the presence of polyethylenglycol (PEG) as the sacrificial template [24]. Due the TMOS sol–gel transition, phase separation occurs between the silica gel network and the polymer. PEG also acts as a carrier of TiO_2 particles into the macropores of silica matrix. In order to disperse TiO_2 nanocrystals in the PEG phase, the oxide particles were functionalized with carboxylic acid or amine derivatives [25], which make the TiO_2 surface less hydrophilic, improving the interactions with the polymeric chains. Subsequent annealing at 500 °C removes both PEG and functionalizing organic molecules and generates the interconnected macroporous silica network. Thus, the TiO_2 crystals, previously dispersed in the PEG phase, graft onto the silica surface channels preserving their crystal phase and size.

TS composites were prepared by using anatase nanoparticles with known morphological and structural characteristics and high photoactivity [3a,3b,26], which were functionalized by carboxylic acid and amine derivatives having different side chains (propionic acid, exylamine and 2-methoxyethylamine). The influence of the functionalizing agent on the dispersion of TiO_2 nanoparticles in PEG and, consequently, on their final exposure and dispersion on silica macropore walls was demonstrated.

Photocatalytic activity of TS samples was tested in the degradation reaction of PhOH in aqueous solution and compared to the same anatase in slurry. It turned out that the immobilization procedure uncommonly preserves the catalytic properties of the TiO_2 nanocrystals.

The proposed new synthetic strategy may be potentially applied to graft different functional oxides to ceramic macroporous substrates, keeping high functional properties eventually modulating the porous architecture of the silica matrix by changing the sol–gel synthesis parameters.

2. Experimental

2.1. Chemicals

All chemicals and solvents were purchased from Sigma–Aldrich as analytical grade and used as received without further purification. Deionised water (18 MΩ cm) was used for the procedures that required water.

2.2. Functionalization of TiO_2 nanoparticles

Nanocrystalline TiO_2 anatase was obtained by hydrothermal synthesis, according to a previously reported procedure [26], by reacting aqueous solutions of $TiOCl_2$ (Aldrich, 99%) and NH_3 (Fluka, >25 wt %) in a teflon lined autoclave (Parr, model 4768Q). The autoclave was heated at a rate of 2.67 °C/min just to 30 °C below the set-point temperature, then at a rate of 0.75 °C/min up to 220 °C. TiO_2 surface was functionalized following a modified literature procedure [25]. In anhydrous conditions, 20 mL of the organic reagent (propionic acid, PA; exylamine, EA; 2-methoxyethylamine, MA) was added to 3.30 g of TiO_2 suspended, after ultrasound treatment, in 40 mL of anhydrous methanol. The amount of the organic reagents was in large excess compared to the oxide. The obtained suspensions were refluxed for 8 h and kept overnight under stirring at room temperature (RT). Finally, the suspensions were divided into 6 aliquots and the particles were separated by centrifugation at 6000 rpm for 30 min and recovered by decantation. In order to remove the unreacted chemicals and the residual traces of methanol, each aliquot was washed for 30 min under ultrasound conditions by ethyl acetate (2 times with 10 mL) and CH_2Cl_2 (2 times with 10 mL), respectively. After each washing treatment, the surnatant was separated by centrifugation and decantation. The final wet powders were dried in air at RT overnight, and the residual solvent evaporated 24 h in vacuum (10^{-2} Torr).

2.3. Preparation of TiO_2–SiO_2 (TS)

TS was prepared by using differently functionalized TiO_2 nanoparticles, obtained as previously described. The whole synthesis procedure of TS is shown in Scheme 1. Specifically 0.723 g of polyethylene glycol (PEG 20000) were dissolved in a water solution of acetic acid (6.90 mL, 0.10 M) under magnetic stirring. After the completed dissolution of the polymer, 150 mg of functionalized TiO_2 particles (TiO_2-PA; TiO_2-EA; TiO_2-MA), corresponding to a nominal content of the 10.7% (w/w) on the final TS material, were added and uniformly dispersed under ultrasound (2–3 min) treatment. Then, 3.10 ml (3.17 g) of TMOS were added to the PEG/TiO_2 mixture and stirred for 5 min at RT. Sol–gel transition was induced by storing the samples in closed vessels at 40 °C for 24 h and, subsequently, at 80 °C for 24 h than removed the surnatant and rinsed the obtained gel with water (3 times with 20 ml). The gel was aged and dried heating in open vessel at 100 °C for 24 h. TS material was successively dried at 150 °C for 1 h and calcined in air at 500 °C for 5 h. The final calcination was also performed at 600 °C, 700 °C, 800 °C and 900 °C in order to study the effect of the annealing temperature on the material structure and morphology (e.g. porosity, surface area, titania crystal phase and size) and on the photoactivity. TS was also prepared by using pristine anatase, according to the same described procedure. TS samples from TiO_2-PA, TiO_2-EA and TiO_2-MA and from pristine TiO_2 are labelled TS-PA, TS-EA, TS-MA and TS-UC, respectively.

2.4. Morphological and chemical characterization

X-ray diffraction (XRD) patterns of the powders were collected with a Brucker D8 Advance (Cu K_α radiation) in the range 20–60°

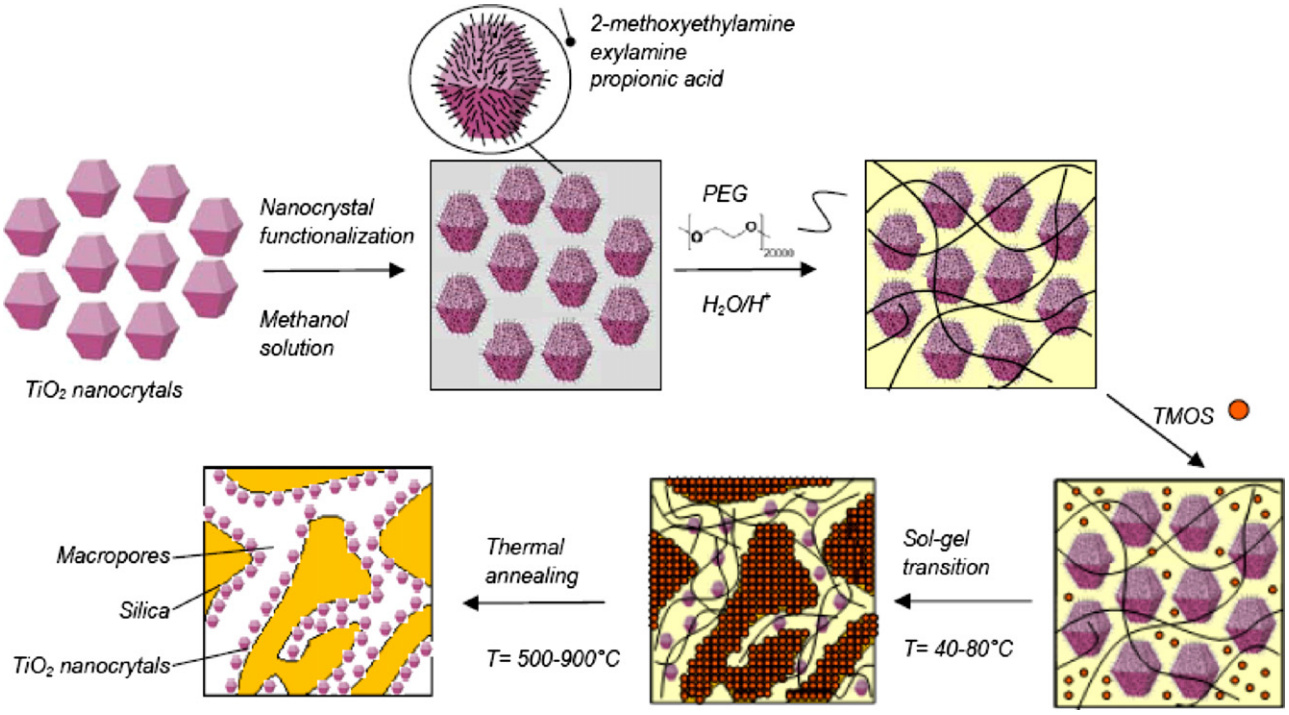

Scheme 1. Overall synthesis process.

2θ (2θ step 0.025°, count time of 2 s per step). TiO_2 nanoparticles functionalized with organic molecules were characterized by ATR-FTIR and Solid-state NMR. ATR-FTIR analysis was performed by a Perkin Elmer Spectrum 100 instrument (1 cm^{-1} resolution spectra, 650–4000 cm^{-1} region, 16 scans). Solid-state NMR analyses were carried out with a Bruker Avance 400WB NMR spectrometer operating at a carrier frequency of 400.13 MHz for ^1H. ^{13}C NMR spectra were acquired with cross-polarization and under the following conditions: ^{13}C frequency, 100.06 MHz; $\pi/2$ pulse length, 2.8 μs; ^1H decoupling pulse power, 47 kHz; recycle delay, 5 s; contact time during CP, 2 ms; number of scans, 14,000. Samples were packed in 4 mm zirconia rotors, which were spun at 8 kHz under air flow. Adamantane was used as secondary reference. Quantitative determination of the amount of organic molecules which functionalizes the oxide, was performed by Thermo Gravimetric Analysis (TGA) and Differential Scanning Calorimetry (DSC) measurements performed with a Mettler Toledo TGA/DSC1 STAR^e System, at constant gas flow (50 cm^3 min^{-1}). Thermal profile was the following: 40 °C 5 min (under N_2); 40–150 °C 10 °C min^{-1} (under N_2); 150 °C 5 min (under N_2); 150–1000 °C 10 °C min^{-1} (under air). The size distribution of macropores (>50 nm) was measured by mercury porosimetry with a Pascal 140/240 Thermo Fisher instrument, assuming 140° as contact angle between mercury and sample. The pressure range varied between 15.8 kPa and 200 MPa.

Specific surface area (SSA) by BET method [27], desorption cumulative pore volume (DCPV) and pore size distribution of micro- and mesopores (<50 nm) by BJH method [28] were measured by nitrogen physisorption using Quantachrome Autosorb-1 apparatus. Powder samples were evacuated at 200 °C for 16 h before the analysis. Scanning electron microscopy (SEM) measurements were performed by a LEO 1450VP instrument. Transmission Electron Microscopy (TEM), High-Resolution Transmission Electron Microscopy (HRTEM) and Electron Diffraction (ED) measurements were performed using a Jeol 3010 apparatus operated at 300 kV with a high-resolution pole piece (0.17 nm point to point resolution) and equipped with a Gatan slow-scan 794 CCD camera. The powders were suspended in isopropanol, and a 5 μL drop of this suspension was deposited on a holey carbon film supported on 3 mm copper grid for TEM investigation.

2.5. Photocatalytic experiments

Photodegradation experiments were carried out in a specifically designed discontinuous batch photoreactor, described in a previous study [20]. The reactor (600 mL), provided with an external cooling jacket, was equipped with a UV 125 W high pressure Hg arc lamp and placed in a coaxial quartz cylinder without optical filter. Photocatalytic tests were performed in aqueous solution by using O_2 as oxygen donor and operating either with TS materials or with pure TiO_2 powder slurries as catalysts. Approximately 1.20 g of TS (TiO_2 loading 0.128 g, corresponding to 0.21 g L^{-1}) were grossly moulded and dispersed in 600 mL of phenol (PhOH) aqueous solution (121 ± 2 mg L^{-1} of PhOH, 93 ± 2 mg L^{-1} as C). The obtained mixture was recirculated by a peristaltic pump with a speed of 14 mL s^{-1}. TS samples were moulded to have the same hydrodynamic conditions of the pure titania used as slurry in photocatalytic experiments.

In the case of pure titania slurry, TiO_2 powder (160 ± 5 mg; 0.25 g L^{-1}) was suspended by sonication in 600 mL of water containing the same concentration of PhOH and recirculated at the same conditions as in the experiments with TS. The reaction was performed at 25 ± 2 °C, by keeping the oxygen feed constant and by eliminating the excess of gas through a non return check valve. The dissolved oxygen content was monitored by an online sensor. The slurry was circulated in the dark and saturated in an online chamber by continuously bubbling oxygen (100 mL min^{-1}). The oxygen content became maximum and constant in about 10 min. The UV source was turned on after 1 h of recirculation in the dark. The PhOH adsorption on the catalyst was checked by withdrawing suspension aliquots (6 mL) of the solution at regular intervals and analyzing the TOC by a Shimadzu TOC-V CSH analyzer. Powders were separated by centrifugation before TOC analysis. The same procedure was applied to monitor the kinetics until the complete mineraliza-

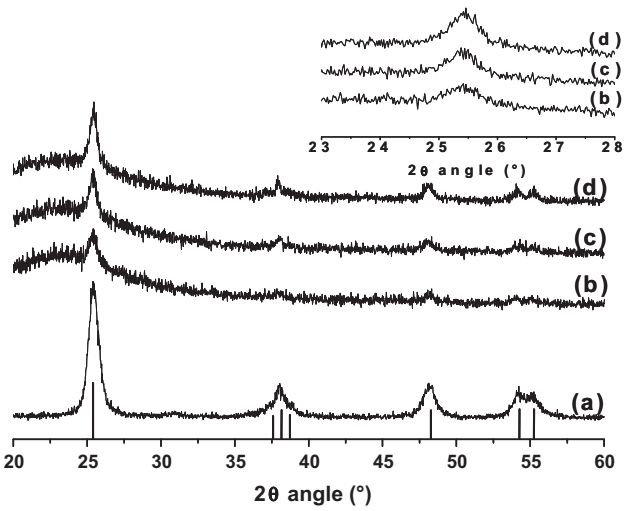

Fig. 1. XRD powder pattern of (a) anatase powder and TS-MA calcined at (b) 500 °C, (c) 700 °C and (d) 900 °C. Inset: magnification of (1 0 1) peak. The vertical lines indicate position and intensities of anatase reflections.

tion of the substrate. Finally, reference experiments (Blank) were carried out in the absence of TiO_2 and TS.

3. Results and discussion

3.1. Characterization of pristine and functionalized TiO_2 nanoparticles

The XRD pattern of pristine anatase TiO_2 nanoparticles is reported in (Fig. 1). The average crystallite size, estimated from the peak of (1 0 1) reflection using Scherrer's equation, resulted 10.5 nm. The XRD patterns (not reported) of TiO_2-PA, TiO_2-EA, TiO_2-MA, TiO_2 functionalized with propionic acid, exylamine and 2-methoxyethylamine respectively, revealed the same size and phase of the pristine TiO_2 nanoparticles.

TiO_2-PA, TiO_2-EA, TiO_2-MA nanoparticles were characterized by means of solid-state ^{13}C NMR and ATR-FTIR. The obtained NMR spectra assessed the effective functionalization of the anatase surface (Fig. 2). The detected ^{13}C signal peaks were assigned according to the literature values [29] and are summarized in Table 1.

The ^{13}C NMR spectra of TiO_2-EA and TiO_2-MA exhibit the signals due to hexylamine and 2-methoxyethylamine, respectively (Table 1). In particular, the two different signals in the TiO_2-EA spectrum attributed to carbon C-6, are explained by the γ-gauche effect [30]. The hexylamine chains can exist in two stable conformations, i.e. *trans* and *gauche* states of the C-4–C-5 bond, which cause different electronic shielding at carbon C-6. Accordingly, the gauche conformation induces an upfield shift of the ^{13}C resonance compared to the trans one. It is assumed that the attachment of the chains to the anatase surface freezes the two conformational states on the NMR timescale, and the different conformations give rise to two different resonances of carbon C-6.

This behaviour is not detected in the TiO_2-MA sample, where the MA chain is too short to exhibit such a conformational effect.

The ^{13}C NMR spectrum of TiO_2-PA shows the signals of methyl and methylene groups of PA (Table 1). The lack of C=O peaks can be ascribed to the poor signal-to-noise ratio and to the large chemical shift anisotropy, which causes spinning sidebands and a distribution of the overall intensity over several signals resonances. Moreover, for carbonyl groups the signal enhancement due to ^{13}C–^{1}H cross-polarization is rather limited due to the lack of directly bonded protons. In TiO_2-PA spectrum, the observed ethyl acetate signals are due to traces of residual washing solvent.

FTIR spectra of TiO_2-PA, TiO_2-EA, TiO_2-MA, compared to those of PA, EA and MA and of pristine anatase, are shown in Fig. S1 (Supporting Information).

The spectra confirm the grafting of the organic molecules on titania nanoparticles in agreement with the ^{13}C CPMAS NMR results. In TiO_2-PA, the PA grafting is demonstrated by the presence of the carboxylate stretching modes and the disappearing of the carbonyl stretching one. In TiO_2-MA and TiO_2-EA, the EA and MA surface interactions are evidenced by the bands assigned to the amino groups linked to the acid surface sites of the oxide (band assignment in Supporting Information). The presence, in spite of the repeated washing cycles, of the C–H stretching modes due to the side chains of PA, EA and MA supports the formation of chemical bonds between the functionalizing molecules and TiO_2 nanoparticles in all the examined samples.

The number of functionalizing molecules linked to the anatase nanocrystals (Table 2) was evaluated by thermogravimetric weight

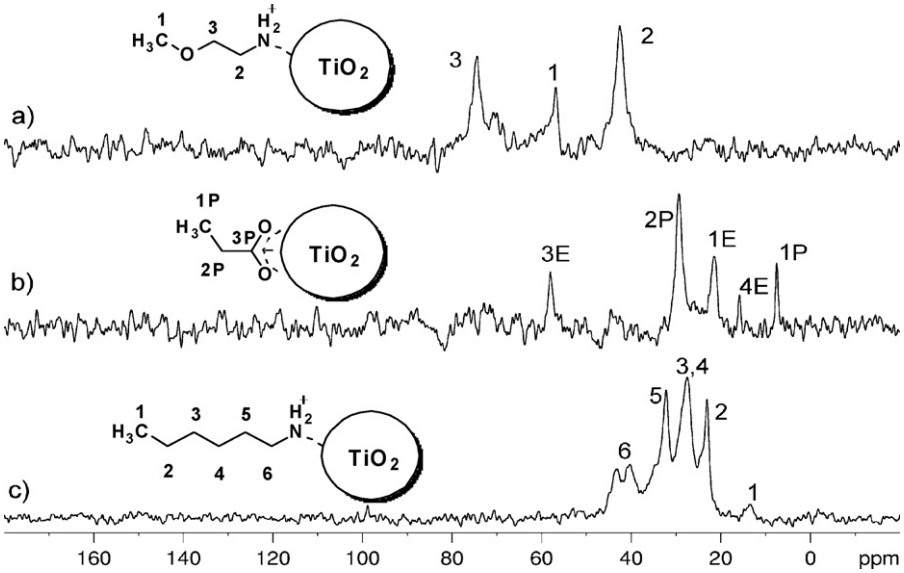

Fig. 2. ^{13}C CPMAS NMR spectra of (a) TiO_2-MA, (b) TiO_2-PA with residues of ethyl acetate and (c) TiO_2-EA. Molecular structures and peak assignment, as reported in Table 1, are shown.

Table 1
^{13}C chemical shifts and signal assignments.

Unit	TiO_2-PA	Ref.	Unit	TiO_2-EA	Ref.	Unit	TiO_2-MA	Ref.
1 [P]	7.5	8.9	1 [H]	13.5	14.1	2 [M]	42.6	41.8
4 [E]	15.8	14.3	2 [H]	23.1	22.8	1 [M]	57.0	58.7
1 [E]	21.7	21.0	3 [H]	27.5	26.7	3 [M]	74.4	74.9
2 [P]	29.4	27.6	4 [H]	28.7	31.9			
3 [E]	58.1	60.4	5 [H]	32.2	34.1			
3 [P]	[nd]	181.5	6 [H]	40.2;43.2	42.4			
2 [E]	[nd]	171.1						

[P], propionic acid; [E], ethyl acetate; [H], n-hexylamine; [M], 2-metoxyethylamine; [nd], not detected.
The reference values are from liquid NMR studies of the pure species [20].

Table 2
Surface density of functional molecules on titania nanoparticles.

Functionalizing agent	MW [g mol^{-1}]	Net loss [weight %]	Σ [mol nm^{-2}]	D [nm]
Propionic acid	74.1	1.18	0.60	1.46
Exylamine	101.2	3.31	1.25	1.01
2-Methoxyethylamine	75.1	1.72	0.86	1.22

loss in the interval 150 °C < T < 600 °C (Fig. S2, Supporting Information), due to the combustion of the organic species. The amount of the functionalizing molecules, expressed as weight %, was calculated by the net weight loss of surface functionalized TiO_2, i.e. the total weight loss, excluding that of bare TiO_2. The density of surface molecules Σ [mol nm^{-2}] was calculated by using the BET Specific Surface Area value of bare anatase (162 $m^2\,g^{-1}$). Finally, the distance between the functionalizing molecules $D = (4/\pi\Sigma)^{1/2}$ [nm] was estimated. The results show that both surface density and distance of the linked molecules are in agreement with the literature data of similar systems [31].

The ability of functionalized particles to be dispersed in organic matrices was tested by simply mixing pristine TiO_2, TiO_2-PA, TiO_2-EA and TiO_2-MA with water and diethyl ether. The mixture water/diethyl ether was chosen to simulate the conditions of the sol-phase, assimilating the water to the aqueous solution of TMOS and the diethyl ether to the PEG phase. Fig. 3 shows the better dispersion of TiO_2-MA particles (d) in the ether phase compared to TiO_2-EA (c) which tends to segregate in the organic phase while TiO_2-PA (b) and bare TiO_2 (a) form homogeneous dispersions in the aqueous phase. This behaviour suggests that the short chain of PA is not able to confer enough hydrophobicity to TiO_2 nanoparticles to be dispersed into organic solvent, unlike TiO_2-EA and TiO_2-MA which have longer chains. In addition, TiO_2-MA nanoparticles are better dispersed in diethyl ether than TiO_2-EA, due to the presence of ether group, which makes them more similar to the solvent as for the polar character.

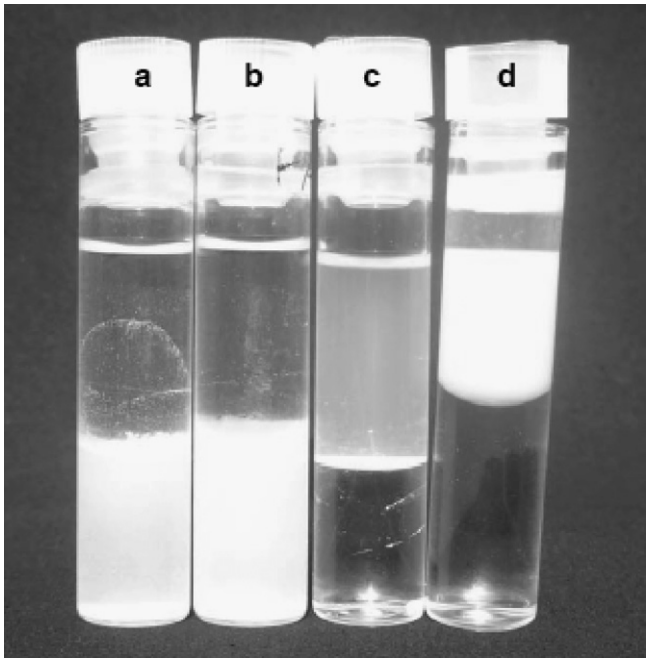

Fig. 3. Test tubes containing ≈10 mg of (a) bare titania; (b) TiO_2-PA; (c) TiO_2-EA and (d) TiO_2-MA in water/diethyl ether mixture.

3.2. Morphological and structural characterization of TiO_2–SiO_2 samples

Macroporosity of TS-MA, TS-PA, TS-EA and TS-UC materials, calcinated at 500 °C were measured by Hg porosimetry. The dimension and the size distribution of the macropores are similar for all samples and not depending on the functionalizing molecules. 60% of the macropores have an average pore radius in the range 0.82–1.21 μm, while the total porosity is about 75 ± 5% of the total volume. TS-MA macropore distribution is shown as example in Fig. S3 (see Supporting Information).

SEM analysis shows that the average size of silica particle in the matrix in all TS samples is about 2.5 μm and confirms the interconnected macroporous structure whose dimensions are in agreement with the porosity measurements (Fig. 4a, sample TS-MA reported).

TEM and HRTEM micrographs demonstrate that TiO_2 nanocrystals are grafted on the surface of silica channels, the exposure and dispersion of the TiO_2 crystallites on silica depending on the side chain of the functional molecules and on their affinity with the PEG. The best result in terms of TiO_2 distribution was obtained for TS-MA, where TiO_2 crystals maintain the size of pristine anatase and interact with the ceramic surface without forming large aggregates (Fig. 4b–d). Comparison of the different samples (Fig. 5) reveals a relevant influence of the functionalizing molecules used on the TiO_2 crystallite dispersion.

In the absence of functionalizing molecules (TS-UC), TiO_2 particles are almost totally embedded in the silica matrix (Fig. 5a). In TS-PA, TiO_2 particles are only partially located on the silica surface (Fig. 5b), while in TS-EA, TiO_2 crystallites form large superficial aggregates (Fig. 5c) instead absent in TS-MA (Fig. 5d), as shown in Fig. 5d or more clearly in Fig. 4c and d.

The different morphology of the materials may be related to the different chains of the functionalizing molecules and to their affinity with PEG. In particular, differently from the case of exylamine and 2-methoxyethylamine, the surface modification induced by the short side chains of propionic acid prevents a suitable dispersion of

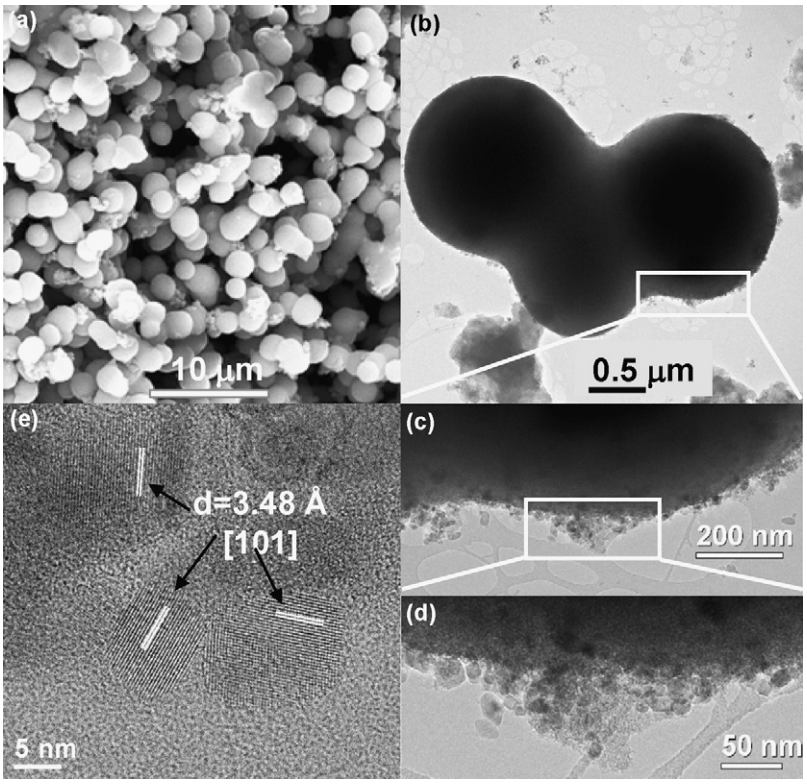

Fig. 4. (a) SEM, (b–d) TEM and (e) HRTEM images at different magnifications of TS-MA after calcination at 500 °C.

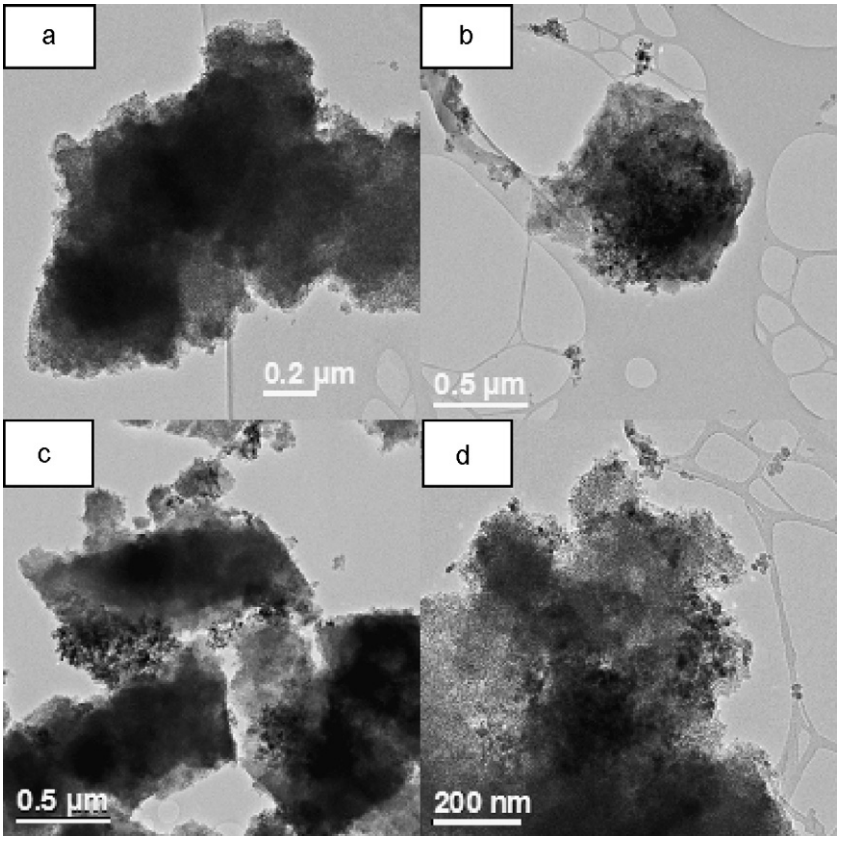

Fig. 5. TEM image of different TS materials calcinated at 500 °C: (a) TS-UC, (b) TS-PA; (c) TS-EA; (d) TS-MA.

TiO_2 nanoparticles into the organic PEG phase during the sol formation. Consequently, PEG is not able to drive TiO_2-PA particles into the silica macropores and to avoid their embedding. Besides, the affinity of the methoxy group of MA with PEG is higher than that of the alkyl chain of exylamine. This implies that TiO_2-MA particles remain well dispersed without secondary aggregation in the PEG phase. On the other hand, the TiO_2-EA particles are both incompatible with the silica phase and not well dispersible by PEG resulting in secondary particle aggregations. The effect of the temperature on the stability and morphology of the TS structure was investigated by annealing TS-MA samples at 600, 700, 800, and 900 °C. XRD diffraction (Fig. 1b–d) and HRTEM analysis evidence that supported TiO_2 also maintains the anatase phase at the highest temperature treatment, wherein the anatase-rutile transition usually occurs [32]. Moreover, the average size of the particles does not substantially change (Fig. 1 inset) even at 900 °C. These effects can be ascribed to the distribution and grafting of titania nanoparticles on the silica surface, preventing either crystal growth or phase transformation usually due to oriented attachment of primary anatase nanocrystals [26].

Finally, at each temperature, no modifications of the macroporous structure were detected, as revealed by Hg porosimetry and SEM analysis (not reported).

Nitrogen physisorption experiments were performed on the pure silica host and on all TS materials. In particular, the adsorption–desorption isotherms and the corresponding pore-size distribution of TS-UC (pseudo-type I) and of TS-MA (type IV) are shown in Fig. 6. The isotherms of TS-UC display high adsorption at low relative pressure, typical of a microporous structure (Fig. 6a). At higher relative pressure, between 0.4 and 0.8 P/P_0, the curve exhibits a very small hysteresis loop indicative of the presence of a small amount of mesopores. This is also confirmed by the corresponding pore-size distribution (Fig. 6a inset) in which only a weak peak in the mesopore range appears. Similar isotherms were obtained for pure silica and TS-PA composite (Fig. S4a, Supporting Information). On the other hand, TS-EA and TS-MA, obtained from TiO_2 nanocrystals functionalized with EA and MA, showed significantly different isotherms. In particular, for TS-MA the resulting isotherm is of type IV and presents a wide hysteresis loop suggesting a remarkable contribution of mesopores (Fig. 6b). The pore size distribution (Fig. 6b inset) confirms the existence of mesopores with average pore diameter centered on 3.6 nm. A similar behaviour was observed for TS-EA (Fig. S4b, Supporting Information), which shows an analogous type IV isotherm but with less pronounced hysteresis loop, suggesting a lower presence of mesopores. By increasing the calcination temperature up to 900 °C, the shape of nitrogen adsorption–desorption isotherm changes and becomes similar to that observed for TS-UC with a decreased contribution of the mesopores (Fig. S4c, Supporting Information).

In order to better elucidate the relation between porosity and structure of the functionalizing molecules, the mesopore and micropore volumes of the pure silica and of the composites were calculated and reported in Fig. 7. It is very evident that the micropore volume, mainly associated to the silica matrix, remains quite constant in all the samples while there is a huge increase of the mesopore volume in TS-EA and TS-MA compared to the value calculated for TS-UC. On the contrary, TS-PA keeps the mesopore volume unvaried in comparison to TS-UC. Finally, the increase of the calcination temperature to 900 °C in TS-MA produces a relevant but not drastic reduction of the mesopore volume, probably due to the growth of nanoparticle aggregates.

These results confirm the key role of the TiO_2 functionalization in controlling the extent of mesoporosity of the composite materials, in agreement with the corresponding TEM images. In TS-MA, titania nanocrystals well dispersed on the silica surface without

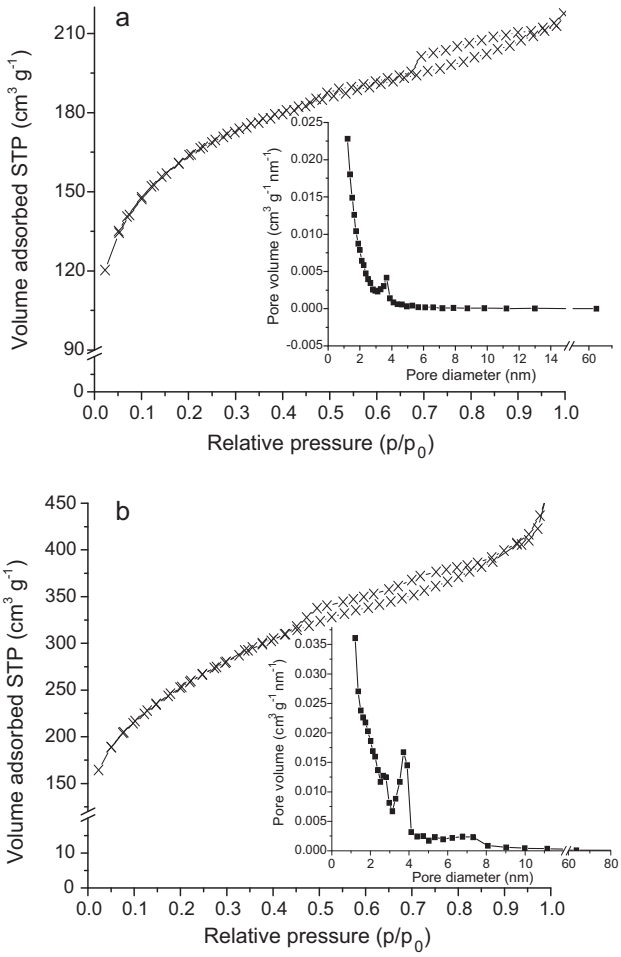

Fig. 6. Adsorption/desorption isotherms at liquid nitrogen temperature for (a) TS-UC and (b) TS-MA samples. The curves correspond to a pseudo-type I (a) and type IV (b) isotherms with capillary condensation in the mesopores. Inset: pore size distributions.

secondary aggregation (Fig. 5d), originate intra-grain mesoporosity. The lower mesoporosity of TS-EA is relatable to the tendency of TiO_2 crystallites to form large superficial aggregates (Fig. 5c). The very low mesoporosity of TS-PA and TS-UC, similar to that of the pristine silica, depends on TiO_2 nanoparticles fairly totally embedded in the silica matrix (Fig. 5a).

3.3. Photocatalytic tests

The photocatalytic activity of TS samples obtained by differently functionalized anatase nanocrystals was measured in the PhOH mineralization in the presence of O_2 under UV radiation and compared to the powder anatase in slurry. The catalyst activity was evaluated by measuring the maximum degradation rate $(dC/dt)_{max}$, which corresponds to the maximum slope point of the fitted curves and the half degradation time ($t_{1/2}$). Both $(dC/dt)_{max}$ and $t_{1/2}$ values were normalized to the same mass (160 mg) of TiO_2.

The experimental data related to TOC disappearance of PhOH mineralization, for TS samples and slurry, are reported in Fig. 8, where 100% TOC at $t = 0$ is the PhOH concentration measured just before switching on UV irradiation. In all the performed experiments, during the initial phase of recirculation in dark (30 min), the loaded PhOH concentration decreased by about $5.0 \pm 1.5\%$.

The trends of the calculated values of $t_{1/2}$ and $(dC/dt)_{max}$ are reported in Fig. 9a.

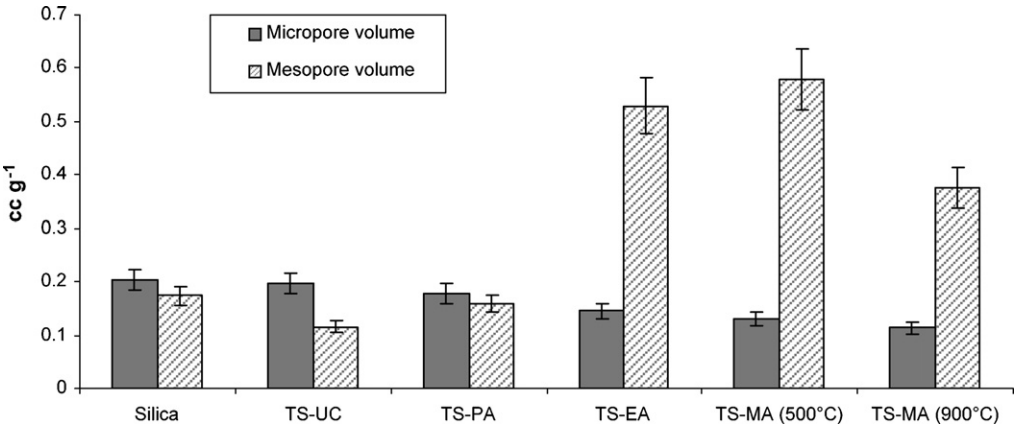

Fig. 7. Mesopore and micropore volumes calculated by the BJH method for pure silica and different TiO_2–SiO_2 samples.

In the blank test, without the catalyst, the PhOH mineralization rate is very low, thus indicating a negligible contribution of the direct PhOH photolysis to the whole process. The overall results evidence that the photoactivity of TS compounds is strongly related to the nature of the functionalizing molecules. In particular, $t_{1/2}$ value decreases and $(dC/dt)_{max}$ correspondingly increases by increasing the chain length of the molecules as well as their affinity with PEG. In particular, TS-PA and TS-UC display the lowest photoactivity, while TS-EA and TS-MA show higher efficiencies. Surprisingly, TS-MA shows the same performance of anatase slurry, thus demonstrating that the TiO_2 immobilization procedure did not affect its catalytic properties. This behaviour can be related to the high catalyst dispersion of anatase nanocrystals on the surface of silica macropores which induces extended mesoporosity in TS-MA composite. These properties guarantee high accessibility of the catalyst at the solid liquid interface and an intimate contact between the target molecules and the nanoparticles.

The photocatalytic tests were repeated for six successive degradation runs with the same batch, in order to validate the reproducibility of the TS-MA catalytic behaviour. Photoactivity remains substantially constant as demonstrated by the negligible variation of the $t_{1/2}$ (Fig. 9b) and $(dC/dt)_{max}$ (not reported in the figure) calculated for the successive runs.

Finally, the different calcination temperatures have a minor effect on the catalytic properties of TS-MA, as assessed by the very slightly increase of $t_{1/2}$ values with the temperature (115 ± 6 min, 125 ± 6 min and 133 ± 7 min for calcination temperature of 500 °C, 700 °C and 900 °C, respectively) and by the constancy of $(dC/dt)_{max}$ ($0.42 \pm 0.02\ min^{-1}$). The overall results confirm that even at highest calcination temperatures morphology of silica, TiO_2 phase and TS-MA composite porosity (see Section 3.2) are substantially unchanged preserving the photoactivity.

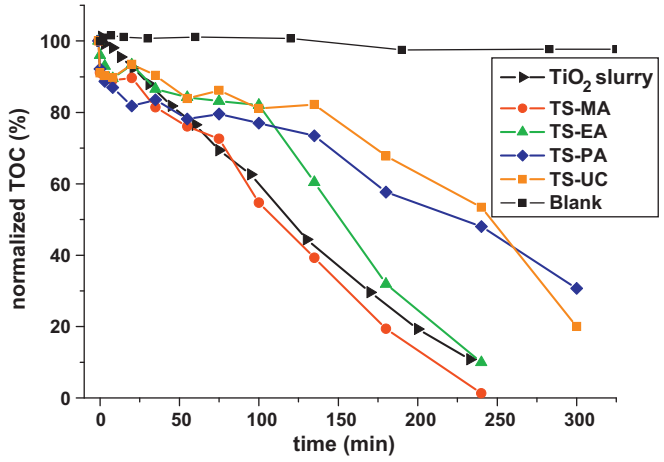

Fig. 8. Mineralization curves of phenol (given as TOC %) in the presence of O_2 of TS-PA, TS-EA, TS-MA and TS-UC samples compared with TiO_2 catalyst in slurry and with the blank test without catalyst.

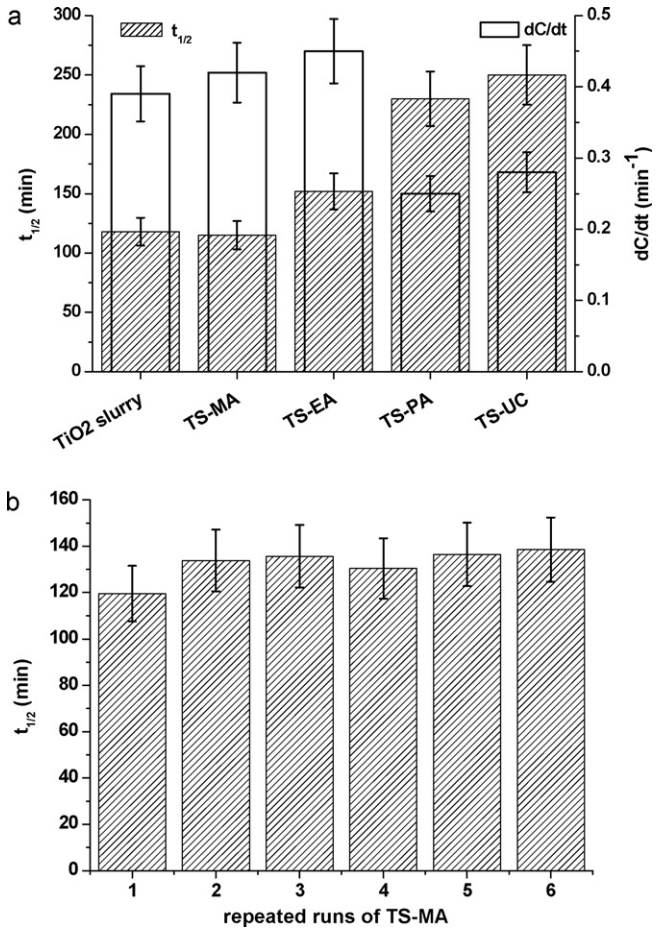

Fig. 9. (a) Maximum degradation rate $(dC/dt)_{max}$ and half degradation time ($t_{1/2}$) of different TS materials compared with TiO_2 catalyst in slurry; (b) $t_{1/2}$ of TS-MA after six repeated photomineralisation runs.

4. Conclusions

TiO_2–SiO_2 composite materials with nanostructured TiO_2 particles grafted onto macroporous silica support were successfully obtained by a novel sol–gel synthetic strategy which employs hybrid organic–inorganic reactants. The materials exhibits high thermal stability and a photocatalytic activity comparable to that of powder TiO_2 in slurry.

The macroporous silica network was synthesized by hydrolysis and condensation of TMOS assisted by PEG as templating agent. TiO_2–SiO_2 were prepared by grafting preformed titania nanocrystals, suitably functionalized by different organic molecules which facilitate their interaction with PEG, onto the macropores of the silica matrix, avoiding their embedding into the support.

Titania dispersion on the silica surface depends on the chain structure of the functionalizing molecules as well as on their affinity with PEG. In particular, the highest affinity of the methoxy group of 2-methoxyethylamine towards PEG enables TiO_2 nanocrystals to maintain the pristine size and to disperse on the silica surface as small mesoporous aggregates, independently of the calcinations temperature.

The structure of the composites allows high photocatalytic yields. Particularly, TS-MA shows outstanding photoactivity, equal to that of the slurry. This is relatable to the dispersion of anatase nanocrystals on the surface of silica macropores, which induces extended mesoporosity of TS-MA composite. These properties guarantee high accessibility of the catalyst interface and an effective contact between the pollutant molecules and the nanoparticles. The overall results confirm the ability of the immobilization procedure to preserve the functional properties of the photoactive oxide.

Therefore, this highly stable TiO_2–SiO_2 meso/macroporous composite represents a very promising material, easy to be obtained and to be used in various applications. The simplicity of the immobilization method should, in principle, be applicable to support different oxides maintaining unchanged their peculiar functional properties.

Acknowledgements

The Milan group gratefully acknowledge Dr. Paolo Gentile for the SEM images and Dr. Angeloclaudio Nale for the XRD experiments.

Appendix A. Supplementary data

Supplementary data associated with this article can be found, in the online version, at doi:10.1016/j.apcatb.2011.03.018.

References

[1] (a) M.R. Hoffmann, S.T. Martin, W. Choi, Chem. Rev. 95 (1995) 69;
(b) T.T. Thomson, J.T. Yates, Chem. Rev. 10 (2006) 4428;
(c) X. Chen, S.S. Mao, Chem. Rev. 107 (2007) 2891.
[2] (a) P. Salvador, J. Phys. Chem. C 111 (17038) (2007);
(b) U. Diebold, Surf. Sci. Rep. 48 (2003) 53;
(c) P. Davit, G. Martra, S. Coluccia, J. Japan Petr. Inst. 47 (2004) 359;
(d) J. Theurich, M. Lindner, D.W. Bahnemann, Langmuir 12 (1996) 6368;
(e) R. Vinu, G. Madras, Environ. Sci. Technol. 42 (2008) 913;
(f) M. Ampo, T. Shima, Y. Kubokawa, Chem. Lett. 12 (1985) 1799;
(g) K. Okamoto, Y. Yakamoto, H. Tanaka, M. Tanaka, M.A. Itaya, Bull. Chem. Soc. Jpn. 58 (1985) 2015.
[3] (a) R. Scotti, M. D' Arienzo, A. Testino, F. Morazzoni, Appl. Catal. B: Environ. 88 (2009) 497;
(b) R. Scotti, I.R. Bellobono, C. Canevali, C. Cannas, M. Catti, M. D'Arienzo, A. Musinu, S. Polizzi, M. Sommariva, A. Testino, F. Morazzoni, Chem. Mater. 20 (2008) 4051.
[4] (a) R. Molinari, L. Palmisano, E. Drioli, M. Schiavello, J. Membr. Sci. 206 (2002) 399;
(b) W.Y. Wang, A. Irawan, Y. Ku, Water Res. 42 (2008) 4725;
(c) W. Xi, S.V. Geisen, Water Res. 35 (2001) 1256.
[5] L. Reijnders, J. Hazard. Mater. 152 (2008) 440.
[6] M. Tashibi, C.R. Ngah, N. Aziz, A. Mansor, A.Z. Abdullah, L.K. Teong, A.R. Mohamed, Ind. Eng. Chem. Res. 46 (2007) 9006.
[7] J. Fernandez, J. Kiwi, J. Baeza, J. Freer, C. Lizama, H.D. Mansilla, Appl. Catal. B 48 (2004) 205.
[8] (a) J.C. Lee, M.S. Kim, B.W. Kim, Water Res. 36 (2002) 1776;
(b) M.D. Nikolaki, D. Malamis, S.G. Poulopoulos, C.J. Philippopoulos, J. Hazard. Mater. 137 (2006) 1189.
[9] (a) S. Horikoshi, N. Watanabe, H. Onishi, H. Hikada, N. Serpone, Appl. Catal. B 37 (2002) 117;
(b) M.K. Aminian, N. Taghavinia, A. Irajizad, S.M. Mahdavi, J. Phys. Chem. C 111 (2007) 9794.
[10] (a) I.N. Martyanov, N.J. Klabunde, J. Catal. 225 (2004) 408;
(b) M.G. Antoniou, D.D. Dionysiou, Catal. Today 12 (2007) 4215.
[11] (a) Y. Xu, C.H. Langford, J. Phys. Chem. B 101 (1997) 3115;
(b) F. Li, S. Sun, Y. Jiang, M. Xia, M. Sun, B. Xue, J. Hazard. Mater. 152 (2008) 1037.
[12] S.N. Hosseini, S.M. Borghei, M. Vossoughi, N. Taghavinia, Appl. Catal. B 74 (2007) 53.
[13] S.K. Kansal, M. Singh, D. Sud, J. Hazard. Mater. 153 (2008) 412.
[14] T.H. Xie, J. Lin, J. Phys. Chem. C 111 (2007) 9968.
[15] (a) J. Shang, W. Li, Y. Zhu, Mol. Catal. A 202 (2003) 187;
(b) N. Kieda, T. Tokuhisa, J. Ceram. Soc. Jpn. 114 (2006) 42.
[16] H. Chen, S.W. Lee, T.H. Kim, B.Y. Hur, J. Eur. Ceram. Soc. 26 (2006) 2231.
[17] (a) Z. Liuxue, W. Xiulian, L. Peng, S. Zhixing, Surf. Coat. Technol. 201 (2007) 7607;
(b) B. Tryba, J. Hazard. Mater. 151 (2008) 623.
[18] (a) I.R. Bellobono, R. Barni, F. Gianturco, J. Membr. Sci. 102 (1995) 139;
(b) F. Ascari, I.R. Bellobono, P.M. Tozzi, Fresenius Environ. Bull. 12 (2003) 1195;
(c) I.R. Bellobono, F. Ascari, C. Lagrasta, Fresenius Environ. Bull. 12 (2003) 1536.
[19] (a) L.G.A. van de Water, T. Maschmeyer, Top. Catal. 29 (2004) 67;
(b) Y.S. Lin, Sep. Purif. Technol. 25 (2001) 39.
[20] (a) R. Scotti, M. D'Arienzo, F. Morazzoni, I.R. Bellobono, Appl. Catal. B: Environ. 88 (2009) 323;
(b) M. D'Arienzo, M. Crippa, A.A. Essawy, R. Scotti, L. Wahba, P. Gentile, I.R. Bellobono, S. Polizzi, F. Morazzoni, J. Phys. Chem. C 114 (2010) 15755.
[21] (a) Y.H. Wang, X.Q. Liu, G.Y. Meng, Mater. Sci. Eng. A 445 (2007) 611;
(b) M.A. Anderson, M.J. Gieselmann, Q. Xu, J. Membr. Sci. 39 (1988) 243;
(c) F. Bosc, A. Ayral, P.A. Albouy, L. Datas, C. Guizard, Chem. Mater. 16 (2004) 2208;
(d) G. Balasubramanian, D.D. Dionysiou, M.T. Suidan, V. Subramanian, I. Baudin, J.M. Laîneî, J. Mater. Sci. 38 (2003) 823;
(e) P.C.A. Alberius, K.L. Frindell, R.C. Hayward, E.J. Kramer, G.D. Stuchy, B.F. Chmelka, Chem. Mater. 14 (2002) 3284;
(f) S.Y. Kwak, S.H. Kim, S.S. Kim, Environ. Sci. Technol. 35 (2001) 2388.
[22] (a) H. Choi, E. Stathatos, D.D. Dionysiou, Appl. Catal. B: Environ. 63 (2006) 60;
(b) F. Bosc, P. Lacroix-Desmazes, A. Ayral, J. Colloid Interface Sci. 304 (2006) 545;
(c) A. Julbe, V. Rouessac, J. Durand, A. Ayral, J. Membr. Sci. 316 (2008) 176;
(d) H. Bai, Z. Liu, D.D. Sun, Chem. Commun. 46 (2010) 6542;
(e) H. Choi, A.C. Sofranko, D.D. Dionysiou, Adv. Funct. Mater. 16 (2006) 1067.
[23] P. Colombo, C. Vakifahmetoglu, S. Costacurta, J. Mater. Sci. 45 (2010) 5425.
[24] N. Tanaka, H. Kobayashi, N. Ishizuka, H. Minakuchi, K. Nakanishi, K. Hosoya, T. Ikegami, J. Chromatogr. A 965 (2002) 35.
[25] N. Nakayama, T. Hayashi, Colloids Surf. A: Physicochem. Eng. Aspects 317 (2008) 543.
[26] A. Testino, I.R. Bellobono, V. Buscaglia, C. Canevali, M. D'Arienzo, S. Polizzi, R. Scotti, F. Morazzoni, J. Am. Chem. Soc. 129 (2007) 3564.
[27] S. Brunauer, P.H. Emmet, E. Teller, J. Am. Chem. Soc. 60 (1938) 309.
[28] E.P. Barret, L.G. Joyner, P.P. Halenda, J. Am. Chem. Soc. 73 (1951) 373.
[29] (a) D.P. Cistola, D.M. Small, J.A. Hamilton, J. Lipid Res. 23 (1982) 795;
(b) H. Tomita, F. Sanda, T. Endo, J. Polym. Sci. Part A: Polym. Chem. 39 (2001) 3678;
(c) E. Breitmeier, W. Voelter, Carbon 13 NMR Spectroscopy, VCH Verlagsgesellschaft GmbH, Weinheim, Germany, 1987, Ch 2.
[30] (a) A.E. Tonelli, NMR Spectroscopy and Polymer Microstructure: The Conformational Connection, VCH Verlagsgesellschaft GmbH, Weinheim, Germany, 1989, Ch 6;
(b) D.M. Grant, B.V. Cheney, J. Am. Chem. Soc. 89 (1967) 5315.
[31] I. Luzinov, D. Julthongpiput, H. Malz, J. Pionteck, V.V. Tsukruk, Macromolecules 33 (2000) 1043.
[32] C. Byun, J.W. Jang, I.T. Kim, K.S. Hong, B.W. Lee, Mater. Res. Bull. 32 (1997) 431.